Journal of Alloys and Compounds 488 (2009) 638–642

Contents lists available at ScienceDirect

Journal of Alloys and Compounds

journal homepage: www.elsevier.com/locate/jallcom

Correlation between structure variation and luminescence red shift in YAG:Ce

Y.X. Pan[a], W. Wang[a], G.K. Liu[a,*], S. Skanthakumar[a], R.A. Rosenberg[b], X.Z. Guo[c], Kewen K. Li[c]

[a] Chemical Sciences and Engineering Division, Argonne National Laboratory, Argonne, IL 60439, United States
[b] Experimental Facilities Division, APS, Argonne National Laboratory, Argonne, IL 60439, United States
[c] Boston Applied Technologies Ins., 6F Gill St, Woburn, MA 01801, United States

ARTICLE INFO

Article history:
Received 22 June 2008
Received in revised form 3 February 2009
Accepted 16 April 2009
Available online 23 April 2009

Keywords:
YAG:Ce phosphor
5d–4f transition
Lattice expansion
Crystal-field splitting

ABSTRACT

Red shift of Ce^{3+} luminescence in $Y_3Al_5O_{12}$ (YAG) co-doped with Gd^{3+} is investigated with X-ray diffraction (XRD) based structural analysis and crystal-field modeling of electronic energy levels. It shows a linear relationship between the lattice expansion induced by substituting Gd^{3+} for Y^{3+} and the red shift in the Ce^{3+} luminescence. A crystal-field analysis of the Ce^{3+} 5d energy levels is conducted to establish the correlation between the YAG lattice expansion and the Ce^{3+} energy level shifts.

1. Introduction

Phosphor conversion of the UV/blue light emitting diode (pc-LED) radiation into white light emission has been identified as one of promising technologies of solid-state lighting (SSL) for future energy efficient light sources. In comparison with conventional lighting technologies such as fluorescent lamps, white LEDs have advantages of energy saving, long lifetime, while being mercury-free. The current commercial white pc-LEDs are made with a phosphor of Ce^{3+} doped $Y_3Al_5O_{12}$ (YAG:Ce). As a result of the $4f^1$–$5d^1$ electronic transition, Ce^{3+} in YAG can efficiently absorbs blue light from 450 nm to 470 nm and emits a broad band of luminescence in the range of 510 nm to over 600 nm. These spectroscopic properties make YAG:Ce a good phosphor for converting the blue radiation of a LED to white light [1–3]. In pc-LED, white light is created by combination of a part of the blue light from the LED chip and the yellow-red luminescence from the YAG:Ce phosphor. For general application particularly for room lighting, an ideal white light device should accurately simulate the sunlight spectrum in the visible region. However, the color rendering index (CRI) of the current commercial white LED products is not high enough to simulate the sun light because of the lack of red components in the emission spectra of the YAG:Ce phosphor. A practical method to solve this problem is to expand the YAG:Ce emission band or induce a red shift through modifications of the phosphor composition. There are many studies of red shift of the YAG:Ce luminescence induced by modification of the YAG composition with substitution of Y^{3+} in the YAG lattice with Gd^{3+} or other trivalent ions with an ionic size larger than that of the Y^{3+}. With such a modification, the Ce^{3+} emission spectrum can be shifted by more than 30 nm toward the red region [4–7]. In the present work, we report experimental results of the structure characterization and spectroscopic measurements on YAG:Ce modified by Gd^{3+}. Based on these results, we attempt to provide a detailed understanding of the consequences of co-doping Gd^{3+} with Ce^{3+} into the lattice of YAG by crystal-field modeling of the correlation between the co-doping induced lattice expansion and the variation of the crystal-field energy levels of Ce^{3+} in Y(Gd)AG.

2. Experimental

Nanosized Y(Gd)AG:Ce crystals with a general composition of $(Y_{1-x}Gd_x)_3Al_5O_{12}$:Ce were synthesized by a citrate–nitrate gel combustion method as described elsewhere [8]. Briefly, soluble metal citrates and citric acid monohydrate were dissolved and mixed in a mixture of de-ionized water and ethanol. The mixture became viscous and self-propagation combustion was initiated with continuous heating on a hot plate. Phosphor precursors were formed after combustion in a short time. Crystallized phosphors were obtained after sintering the precursors at 850 °C for 4 h under CO atmosphere. A single crystal of YAG:Ce was synthesized at Boston Applied Technologies Ins. XRD measurements were performed with an X-ray diffractometer operating with a Cu Kα radiation Ni filter. The powder phosphors were diluted in a layer of optical epoxy and pasted on a piece of glass. The luminescence spectra and efficiency of the powder phosphors were measured with a photon counting spectrometer connected with a light integrating sphere at room temperature, while the low temperature measurements were carried out using an optical cryostat and a spectrometer connected with a photomultiplier.

* Corresponding author.
E-mail address: gkliu@anl.gov (G.K. Liu).

0925-8388/$ – see front matter © 2009 Elsevier B.V. All rights reserved.
doi:10.1016/j.jallcom.2009.04.082

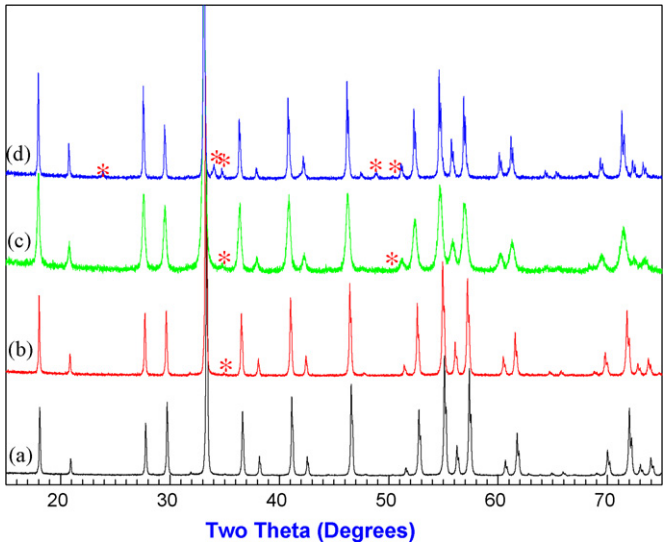

Fig. 1. XRD spectra of $(Y_{1-x}Gd_x)_3Al_5O_{12}$:$Ce_{0.03}$ powder phosphors crystallized at 1200 °C for 2 h. x = 0, 0.03, 0.06, and 0.1, respectively, for samples (a), (b), (c), and (d). Peaks marked by "*" do not belong to the intrinsic YAG structure.

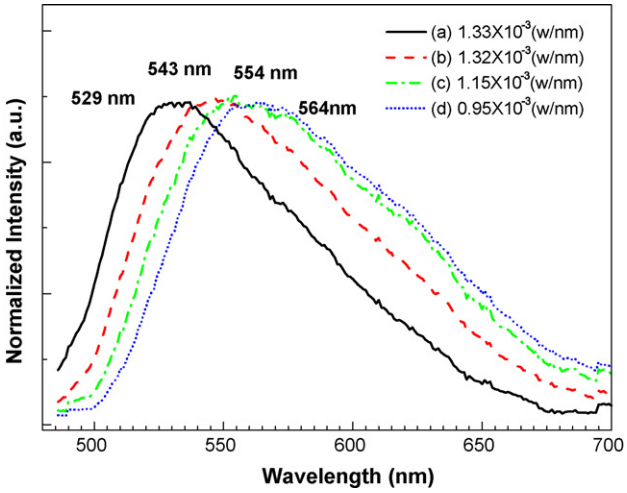

Fig. 2. Red shift and intensity of luminescence from $(Y_{1-x}Gd_x)_{2.97}Al_5O_{12}$:$Ce_{0.03}$ phosphor with composition changes: (a) x = 0, (b) x = 0.03, (c) x = 0.06, and (d) x = 0.1. The spectra for the four samples were obtained with a blue LED with peak at 475 nm excitation and normalized to the peak intensity indicated the legend.

3. Results and discussion

The powder samples of YAG:Ce co-doped with Gd have high quality of crystalline structure. Fig. 1 shows the XRD spectra of $(Y_{1-x}Gd_x)_3Al_5O_{12}$:1%Ce with x varying from 0 to 0.1. No intermediate phase has been observed after the heat-treatment at temperature higher than 850 °C. Based on the XRD data, we have derived the lattice parameters and cell volume (listed in Table 1) of the samples of different Gd concentration. In comparison with the sample without Gd, the peaks shift toward smaller angles with increasing Gd concentration, which is consistent with the observed lattice expansion [4–7]. In addition, minor peaks representing impure phases appear in the samples with a higher Gd concentration. As shown in Fig. 1, $GdAlO_3$ can be identified as an impurity phase in the samples we studied. It is known that the absorption and emission energies of $GdAlO_3$:Ce are much higher respectively than those of YAG:Ce, therefore have no contribution to the luminescence spectrum between 500 nm and 600 nm [9].

The photoluminescence properties of YAG:Ce series powders were investigated to reveal the effects of composition changes on the emission wavelength and the luminescence efficacy. Replacing Y by Gd induces a red shift in the Ce^{3+} emission band as shown in Fig. 2. The normalized emission spectra of the YAG:Ce powders samples with different Gd concentration cover a broad spectral range from 480 nm to 700 nm. The broad Ce^{3+} emission band originates from the 4f–5d electronic transition with intensive side bands due to vibronic coupling to the lattice and local vibration modes in the YAG lattice [10]. As the Gd concentration increasing, the center of the emission band shifts from 529 nm to 564 nm. Such a shift is primarily due to the variation of the lowest crystal-field energy level (emitting state) of the $5d^1$ state which depends strongly on the local electrostatic field determined by the crystalline structure of the YAG lattice.

Because the ionic size of Gd^{3+} and Ce^{3+} is larger than that of the host ion Y^{3+}, substituting Gd^{3+} and Ce^{3+} results in a lattice expansion. When the concentration of Ce^{3+} is low and fixed at a constant, the lattice expansion will depend on the concentration of Gd^{3+}. Measured from the XRD spectra, and shown in Fig. 3, the dependence of the lattice constant value on the Gd^{3+} concentration varied from zero to 10% of Y^{3+} is approximately a linear function. It is also interesting to see that the red shift of the Ce^{3+} emission correlates very well with the lattice expansion (Fig. 3). Based on these observations, we can conclude that within the range of Gd^{3+} concentration less than 10%, the red shift of the YAG:Ce luminescence is predominantly originated from the lattice expansion.

In the framework of crystal-field theory, the electronic energy levels of Ce^{3+} in YAG and their shifts observed in the emission and absorption spectra can be evaluated as a function of spin–orbit coupling and crystal-field interaction expressed in terms of Hamiltonian parameters [11]. Other mechanisms such as electrostatic interaction is absent in the $4f^1$ and $5d^1$ configurations. Whereas the lattice expansion induced energy level shifts should be independent of the spin–orbit coupling, the observed red shifts can be calculated as a function of crystal-field parameters. In the lattice of YAG, Ce^{3+} ions occupy the site of Y^{3+} at a tetragonal symmetry of approximately D_2. Considering the doping induced site distortion, the actual site symmetry of Ce^{3+} may be even lower than D_2. However, the five crystal-field energy levels of $6d^1$ is not sufficient to determine the free-ion and crystal-field parameters for D_2 symmetry especially for B_2^2 and B_2^4. In our calculations, an approximation of D_{2d} is considered. Accordingly, the crystal-field splittings for a

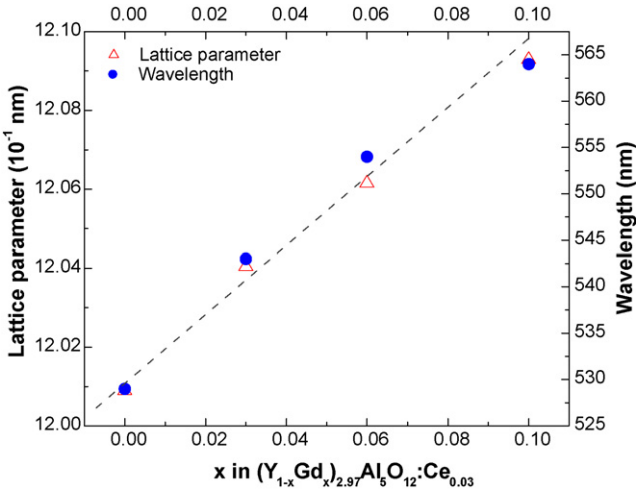

Fig. 3. Comparison of the lattice expansion and the red shift of Ce^{3+} luminescence as function of Gd^{3+} concentration in $(Y_{1-x}Gd_x)_{2.97}Al_5O_{12}$:$Ce_{0.03}$.

Table 1
Lattice expansion, energy level of the 5d emitting state, and 5d crystal-field strength according to Eq. (2) for $(Y_{1-x}Gd_x)_{2.97}Al_5O_{12}:Ce_{0.03}$ are evaluated as a function of Gd concentration (x).

X	Lattice (Å)	Cell volume (Å^3)	Emitting state energy (cm^{-1})	Crystal-field strength (cm^{-1})
0	12.00888	1731.8369	20,450	1892
0.03	12.04047	1745.5421	19,963	2217
0.06	12.06151	1754.7109	19,597	2462
0.1	12.09289	1768.4383	19,277	2677

5d state are determined by [12]:

$$H(5d) = \varsigma_{SO}(d)A_{SO}(d) + B_0^2(d)C_0^{(2)} + B_0^4(d)C_0^{(4)} + B_4^4(d)(C_4^{(4)} + C_{-4}^{(4)}) \quad (1)$$

where the first term is the spin–orbit interaction and $B_q^k(d)$ are the crystal-field parameters for the 5d states and $C_q^{(k)}$ are operators of spherical harmonic functions. Because the 4f states have much weaker crystal-field interaction, one can assume that the observed red shift in the Ce^{3+} 5d–4f transition is dominantly contributed by the energy level shift in the excited 5d emitting state.

In the present work, Eq. (1) is used for evaluating a systematic trend of the changes in the Ce^{3+} energy levels expressed in terms of the crystal-field parameters. In order to establish such a correlation, the observed electronic energy levels must be obtained from absorption and emission spectra of a single crystal of YAG:Ce. In fact, vibronic features dominate the emission and absorption spectra of the 5d–4f transitions. Ion-phonon coupling and structure defects induced inhomogeneous line broadening often obscure the lines of zero-phonon electronic transitions. Only with Ce^{3+} diluted in a single crystal cooled to liquid helium temperature, one may observe the zero-phonon lines. As shown in Fig. 4, two sharp lines with a line width of approximately 20 cm^{-1} located at 489 nm and 546 nm are assigned to the zero-phonon lines from the emitting 5d state to the ground configuration 4f states of $^2F_{5/2}$ and $^2F_{7/2}$, respectively. This result is consistent with the previously reported work by Robbins [13], who clearly resolved the zero-phonon-line (ZPL) of emission spectrum (at 4 K) at 20,441 cm^{-1}, and that of the absorption spectrum at 20,443 cm^{-1}. An intensity profile of mirror symmetry between the emission and absorption suggests the same vibronic coupling in emission and absorption. The band center (or intensity peak) is about 1400 cm^{-1} from the ZPLs. At higher temperature or due to disordering, the first 4f–5d absorption appears at 460 nm, while the emission band centers at 520 nm. However, we should keep in mind that the electronic energy level of the lowest 5d^1 state should be assigned to 489 nm and the same vibronic shift should be subtracted from the other absorption bands when assigning energy levels for other 5d^1 states.

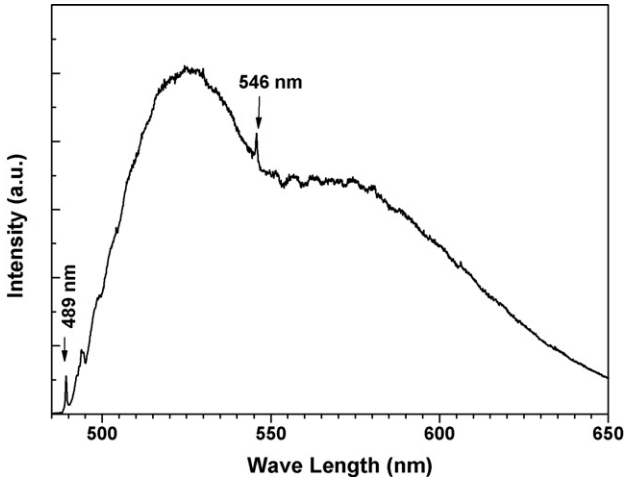

Fig. 4. Emission spectrum of single crystal of YAG:1%Ce^{3+} at 4 K excited by a 475 nm laser beam. The two sharp peaks marked in the spectrum are due to Ce^{3+} 5d^1 zero-phonon transition to the state of 4f^1 $^2F_{7/2}$ and $^2F_{5/2}$, respectively, while the broad band following the zero-phonon lines are vibronic transitions.

Apparently, the energy levels of 5d^1 states of Ce^{3+} in YAG are not clearly understood, even though in the literature there are a number of reports on both experimental investigations and theoretical modeling of the 5d^1 energy level structure for Ce^{3+}:YAG [13–16]. The experimental results from different groups are not quite consistence. The primary difficulty is presumably that the energy span of the 6d^1 states is on the same order or even larger than the energy gap between the valence and conduction bands. It was observed that the ground 4f photoconduction occurs at 30,650 cm^{-1} (3.8 eV) [14], where the energy levels of the upper three 5d^1 states are located in a region from 38,300 cm^{-1} to 48,880 cm^{-1}. Our crystal-field analysis relied on the experimental results from the optical absorption spectra reported by Hamilton et al. [14] and by Tomiki et al. [15]. The band peaks reported by these two groups are consistent where as the upper three bands are resolved more clearly in Ref. [14]. A recent review of experimental results and crystal-field analysis by Tanner et al. [16] proposed three different assignments of the 5d^1 energy level structure. The energy levels in these three assignments are different only for the upper three levels. The values of crystal-field parameters vary significantly for these assignments. In view of energy levels, only the third assignment is more consistent with the experimental results of Refs. [14,15]. This work provided a general insight to the crystal-field splitting of the excited 5d^1 states of Ce^{3+}:YAG. However, the authors apparently assigned the band peaks instead of the ZPLs to the 5d^1 states based on which the crystal-field analysis was performed.

The present work reinvestigated the previous discrepancies in assigning the upper 5d^1 energy levels. Our crystal-field analysis is based on the results from Refs. [14,15] and our own experiment as shown in Fig. 4. Only ZPLs are used in energy level assignment. The ZPL for the lowest level is clearly seen in the emission spectrum (Fig. 4) and in a high resolution absorption spectrum [13] of single crystal samples. The energy difference between the ZPL and the band peak is 1400 cm^{-1}. Therefore, ZPL positions for the upper four levels are determined by subtracting the 1400 cm^{-1} vibronic shift from the energies of the band peaks.

In order to understand the underlying reasons for the luminescence red shift, it is necessary to examine how each of the crystal-field terms in Eq. (1) contributes to the energy level shift. First, the calculated energy levels were fit to the experimentally observed values of ZPLs for the five crystal-field levels of the 5d^1 configuration. The crystal-field and spin–orbit Hamiltonian was diagonalized for the 5d^1 configuration of Ce^{3+} in D_{2d} symmetry. The eigenfunctions in terms of $|J,M>$ and calculated energies of the five crystal-field states of the 5d^1 configuration of Ce^{3+} in YAG have been evaluated and are listed in Table 2. In comparison with crystal-field parameters for Scenario III in the work of Tanner et al. [16], the energy level structure calculated using D_{2d} symmetry is approximately the same as that obtained using D_2 symmetry. This is not surprising because of the small contribution from $B_0^2(d)$ and $B_0^4(d)$. Our calculation also agrees with that of Tanner et al. in which

Table 2
Crystal-field energy, eigenfunction and Hamiltonian parameters for $5d^1$ states of Ce^{3+} in YAG.

Exp. energy (cm^{-1})[a]	Cal. energy (cm^{-1})	Eigenfunction ($\|JM_j>$)
20,445	20,461	−0.6763 |3/2, 3/2> 0.6770 |5/2, −5/2> −0.2905 |5/2, 3/2>
28,039	27,679	−0.7313 |3/2, 1/2> 0.6820 |5/2, 1/2>
36,912	36,785	0.6820 |3/2, 1/2> 0.7313 |5/2, 1/2>
42,961	37,589	0.4686 |3/2, 3/2> −0.8787 |5/2, 1/2>
47,478	45,594	−0.5684 |3/2, 3/2> −0.7304 |5/2, −5/2> −0.3788 |5/2, 3/2>
Parameters (cm^{-1})		$\zeta = 996$, $B_0^2 = -1066$, $B_0^4 = -19, 150$, $B_4^4 = 31, 351$

[a] The first level is obtained from emission spectrum (Fig. 4) and other four are from Refs. [14,15].

the third and fourth levels are close with a separation only about 800 cm^{-1}. However, values of the crystal-field parameters, particularly B_0^4, vary significantly, in order to reduce the third level from above 40,500 cm^{-1} down to 36,900 cm^{-1} to fit the experimental data [14,15].

Rediagonalization of the Hamiltonian was conducted while the value of one of the three crystal-field parameters was allowed to vary. As shown in Fig. 5, the energy level of the Ce^{3+} emitting state exhibits a line dependence respectively on the three crystal-field parameters varied up to 50% from the values for the YAG:Ce without Gd doping. This behavior is understood based on the eigenfunctions and energy splittings list in Table 2 while the energy shift is small in comparison with the gaps to the upper crystal-field states of the $5d^1$ configuration.

The increases in B_q^k indicate an enhancement on the local crystal-field strength for Ce^{3+} in the Y(Gd)AG lattice. This result is consistent with a compress of local lattice surrounding the Ce^{3+} ions when Gd^{3+} ions are added to replace Y^{3+} in the YAG lattice. In addition to the variation of the individual crystal-field parameters, such an effect may be described as a function of crystal-field strength defined as

$$N\upsilon = \left[\frac{1}{4\pi}\sum\frac{(B_q^k)^2}{2k+1}\right]^{1/2}. \quad (2)$$

The crystal-field strength is evaluated for Ce^{3+} in YAG with different Gd^{3+} concentrations and list in Table 1. The leading contribution is from the axial crystal-field term of B_4^4, while the contributions from the other two terms are also included according to the same ratios between the values of the parameters for the system without Gd^{3+} ions. Such a restriction is based on the assumption that the intrinsic symmetry is preserved even though the actual site for Ce^{3+} in YAG:Ce added with Gd^{3+} may have a certain degree of distortion. This assumption is supported by the XRD spectra as shown in Fig. 1 and the linear variation of the parameters shown in Fig. 5. In fact, this behavior is expected because the number of Gd^{3+} ions substituting for Y^{3+} is small and does not change the site symmetry of Ce^{3+} and the related crystalline properties.

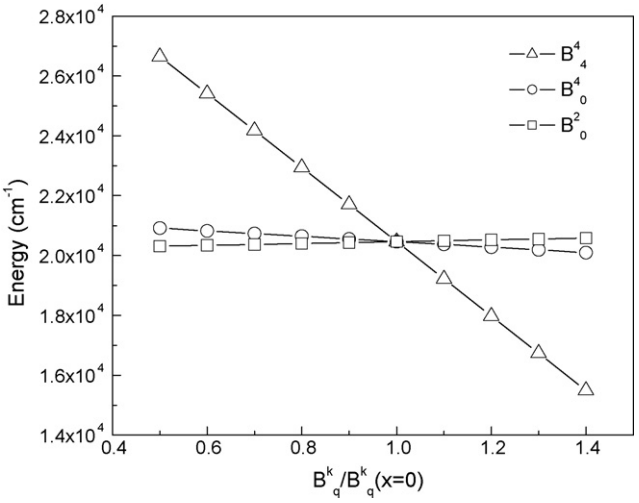

Fig. 5. Dependence of the energy level of the $5d^1$ emitting state on the model crystal-field parameters for Ce^{3+} in YAG:Ce modified by Gd^{3+}. $B_q^k(x=0)$ are the 5d crystal-field parameters of Ce^{3+} in YAG without Gd doping. Their values are listed in Table 2.

It is previously reported and also observed in our experiments that increase in Gd^{3+} concentration leads to a decrease of the YAG:Ce luminescence intensity or quantum efficiency [17]. Several mechanisms may be involved for leading to such a decrease, while two of them are obvious and may be dominant. First, lattice expansion from the unperturbed structure of the pure YAG lattice induces a much larger energy shift on the 5d states than on the 4f states. As a result, the 5d–4f electronic transitions become less efficient, or the zero-phonon lines become weaker. This effect is evident in the emission spectrum of YAG:Ce added with a higher concentration of Gd^{3+}, in which the intensity in the short wavelength side dropped significantly but not in the in the red region. Secondly, as we indicated in the previous section that, when the Gd concentration increases, impurity phases such as $GdAlO_3$:Ce appears in the phosphor. These impurity phases do not contribute to the light emission in the 500–600 nm region, but may absorb and scatter the blue pumping light. A more detailed analysis of the co-doping induced luminescence efficiency decrease is needed in future studies.

4. Conclusions

We have investigated the consequences of composition changes in YAG:Ce by substituting Y with Gd, which induces lattice expansion and changes in the local crystal-field interaction of Ce^{3+}. Both the increase in the YAG crystal lattice and the red shift of the Ce^{3+} emission band depend linearly on the Gd^{3+} concentration within a range of 10% of the host lattice ion Y^{3+}. The red shift in luminescence band is dominantly due to the energy level decrease of the 5d emitting state. A crystal-field analysis of the $5d^1$ energy levels of Ce^{3+} in Y(Gd)AG shows that the red shift in luminescence band corresponds to an enhancement on the crystal-field interaction of Ce^{3+} in the YAG lattice. The expansion in the YAG lattice leads to an increase in the crystal-field interaction of Ce^{3+}. The crystal-field modeling of the Gd^{3+} induced red shift in the Ce^{3+} luminescence band also provides a basis for understanding the efficiency decrease in the Gd^{3+} doped YAG:Ce phosphor.

Acknowledgements

Work performed at ANL was supported by the U.S. Department of Energy, Office of Basic Energy Sciences, Division of Chemical Sciences, Geosciences, and Biosciences, under contract DE-AC02-06CH11357.

References

[1] P. Shlotter, J. Baur, Ch. Hielscher, M. Kunzer, H. Obloh, R. Schmidt, J. Schneider, Mater. Sci. Eng. B 59 (1999) 390.
[2] J. Baur, P. Schlotter, J. Schneider, Adv. Solid-State Phys. 37 (1998) 67.
[3] K. Höhn, A. Debray, P. Schlotter, R. Schmidt, J. Schneider, United States Patent (2003) 6,613,247.
[4] C.C. Chiang, M.S. Tsai, M.H. Hon, J. Electrochem. Soc. 154 (2007) J326–J329.
[5] M. Kottaisamy, P. Thiyagarajan, J. Mishra, M.S.R. Rao, Mater. Res. Bull. 43 (2008) 1657.
[6] K. Zhan, H.Z. Liu, Y.T. Wu, W.B. Hu, J. Mater. Sci. 42 (2007) 9200.
[7] Y.X. Pan, M.M. Wu, Q. Su, J. Phys. Chem. Solid 65 (2004) 845.
[8] X.Z. Guo, P.S. Devi, B.G. Ravi, J.B. Parise, S. Sampath, J.C. Hanson, J. Mater. Chem. 14 (2004) 1288.
[9] J.W.M. Verweij, M.Th. Cohen-Adad, D. Bouttet, H. Lautesse, B. Moine, C. Pédrini, Chem. Phys. Lett. 239 (1995) 51.
[10] M. Grinberg, A. Sikorska, S. Kaczmarek, J. Alloy. Compd. 300–301 (2000) 158.
[11] G.K. Liu, in: G.K. Liu, B. Jacquier (Eds.), Spectroscopic Properties of Rare Earths in Optical Materials, Springer–Verlag, 2005, pp. 1–89, Ch. 1.
[12] L. Van Pieterson, R.T. Weigh, Meijerrink, M.F. Reid, J. Chem. Phys. 115 (2001) 9382.
[13] D.J. Robbins, J. Electrochem. Soc.: Solid-State Sci. Technol. 126 (1979) 1550.
[14] D.S. Hamilton, S.K. Gayen, G.J. Pogatshnik, R.D. Ghen, W.J. Miniscalo, Phys. Rev. B 39 (1989) 8807.
[15] T. Tomiki, T. Kohatsu, H. Shimabukuro, Y. Ganaha, J. Phys. Soc. Jpn. 61 (1992).
[16] P.A. Tanner, L. Fu, L. Ning, B. Cheng, M.G. Brik, J. Phys.: Condens. Matter 19 (2007) 216213.
[17] K. Zhang, W. Hu, Y. Wu, H. Liu, Physica B 403 (2008) 1678.